The Sternum as an Electrical Shield

Dorin Panescu[1], Ph.D., FIEEE, Mark Kroll[2], Ph.D., FIEEE, Carlyn Iverson[3], Michael Brave[4], M.S., J.D.

[1]Advanced Cardiac Therapeutics, Santa Clara, CA, [2]University of Minnesota, Minneapolis, MN,
[3]Absolute Science, MN, [4]LAAW International, LLC, Scottsdale, AZ

***Introduction* — The TASER® conducted electrical weapon (CEW) delivers electrical pulses that can temporarily incapacitate subjects. We analyzed the distribution of TASER CEW currents in tissues posterior to the sternum to understand the likelihood of triggering cardiac arrhythmias. We also assessed the electrical 'shielding' effects of the sternum.**

***Methods and Results* — Finite element modeling (FEM) was used to approximate the current density and electric field strength in tissues around the sternum. We analyzed 2 CEW dart deployment scenarios: (a) both darts over the anterior aspect of the sternum; and (b) a CEW dart anterior to the sternum and the other over the abdomen. In both scenarios, the sternum provided significant attenuation of CEW currents. Particularly, both FEMs predicted that the residual electrical current or charge from CEWs would be insufficient to cause either cardiac capture or induction of ventricular fibrillation at locations where cardiac tissue would reside relative to the posterior aspect of the sternum.**

***Conclusion* — The sternum offers significant 'shielding' effect and protects the tissues posterior to it against effects of electrical current flow from anteriorly-placed CEW electrodes.**

I. Introduction

Conducted electrical weapons (CEW) are a popular less-lethal force option for law enforcement. These weapons, such as TASER®CEWs, deliver trains (19 PPS) of 79–125 μC electrical pulses and 56–126 μs duration designed to temporarily inhibit a person's neuromuscular control primarily through motor-nerve mediated neuromuscular activation. These pulses are delivered to the suspect's body through probes or darts tethered to the CEW. After an initial, narrow, 54–57 kV spike, intended to establish a conductive path through suspect's clothing, the CEW delivers a 1400–1750 V voltage peak, which decays towards baseline over the duration of the pulse [1–4].

The occurrence of some law enforcement arrest-related-deaths (ARDs) in close temporal association with the use of CEWs has raised speculation about potential direct electrical stimulation of the heart.

In particular, there have been incidents where CEW darts connected with the subject over the sternum anterior aspect. These locations are closer to the surface of the heart and, hence, have a smaller Dart-to-Heart Distance (DTH). Therefore, it is important to understand whether the sternum sufficiently attenuates the distribution of current density and electric fields so as to shield the heart from any dangerous levels of myocardial stimulation.

II. Methods

We have previously estimated the current density threshold required to induce ventricular fibrillation (VF) at 91 mA/cm^2 [5, 6].This threshold is consistent with data published by others [7–10]. To avoid induction of VF, the CEW current density in the heart volume should be less than 91 mA/cm^2.

The myocyte excitation threshold is reported to be 3.5 V/cm, on average (range 2–5 V/cm), at pulse durations of about 2 ms [11–13]. Adjusting this threshold for the 0.1 ms duration of CEW pulses yields an average excitation threshold of 70 V/cm (range of 40–100 V/cm). In order to determine the likelihood of cardiac capture using CEWs, we will use a worst-case E field threshold of 40 V/cm.

Since our goal was to understand whether the sternum increases cardiac safety by providing shielding effects, we focused our analyses on CEW dart placements located anterior to the subject's sternum. Figure 1 illustrates a CEW deployment scenario with both darts anterior to the sternum. Figure 2 is an illustration of a second scenario with one dart anterior to the sternum and the second dart elsewhere. Since the dart-dart distance, or dart spread, is large enough, for simplification, we considered the second dart located over the subject's abdomen. In both figures, the red dots indicate the CEW dart locations from two incidents with civil litigation. However, we expect the conclusions will hold for at least some other second-dart remote locations.

Two 3-D finite element models (FEM) were used to numerically approximate currents delivered during CEW dart deployments. The results were then compared against the VF and cardiac capture thresholds discussed above.

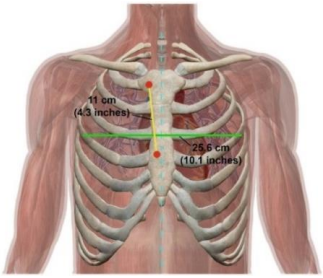

Fig. 1. CEW deployment with 2 darts (red dots) anterior to the sternum.

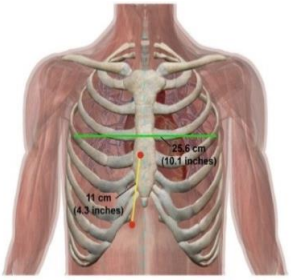

Fig. 2. CEW deployment with 1 dart (red dot) anterior to the sternum.

978-1-4244-7929-0/14/$26.00 ©2014 IEEE

The FEMs had the following characteristics (Figs. 3 and 4):

Tissue regions:
- Epidermis: 2 mm thick
- Dermis: 6 mm thick
- Sternum or Fat: 17 mm thick
- Skeletal muscle or Body tissue: 10 mm thick
- Connective and Cardiac tissue: 10 mm thick
- Models were 22 cm long, 6 cm wide and 4.5 cm thick

General:
- CEW darts were located 11 cm apart and were 4 mm embedded into tissue
- Voltage boundary conditions: 1700 V (TASER®X26™CEW peak voltage [4])
- Models computed steady-state solution

Figures 3 and 4 show 2-D cross-sectional views of the 3-D FEMs. The model consisted of 36,300 hexahedral elements. The FE region resistivities were based on previous published reports (Table I) [5, 6, 8, 14].

TABLE I. FEM MATERIAL PROPERTIES.

Region	Resistivity [Ω·cm]
Epidermis	5000
Dermis	250
Sternum	1000000
Skeletal muscle	$\rho_y = 200$ $\rho_x = \rho_z = 1000$
Connective tissue	500
Broken-down epidermis (conductive spot)	0.001

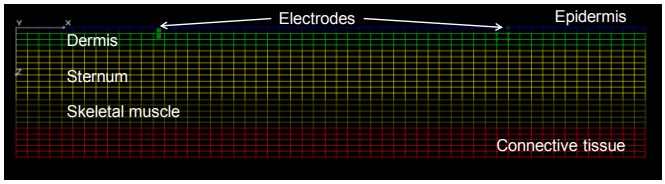

Fig. 3. The FE mesh for deployment with both CEW darts anterior to the sternum.

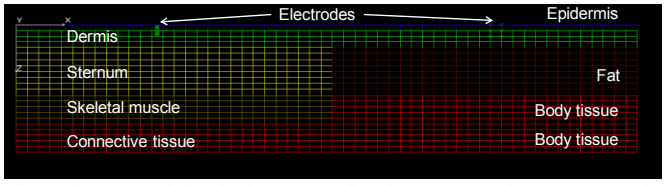

Fig. 4.The FE mesh for deployment with only one CEW dart anterior to the sternum and the second dart over abdomen.

Figure 5 and previous work were used to inspire the FEM dimensions and tissue distributions [5, 6, 8, 15]. For the region modeling the sternum we considered an average thickness of 17 mm, which approximated the average human dimensions [16–18].


Fig. 5. Tissue distribution under sternum for a normal subject [15].

To solve for current density and electric field distributions we used COSMOS [19]. We computed a steady-state solution, as COSMOS can only solve for steady state. However, to account for the worst case scenario, we chose the CEW peak voltage as boundary condition, rather than the average voltage over the pulse duration.

III. RESULTS

With both CEW darts deployed anterior to the sternum, the FEM predicted that the current density will exceed the VF threshold, 91 mA/cm^2, only in the dermis and epidermis regions. Those regions are anterior to the sternum. All regions posterior to the sternum (e.g. where cardiac tissue would be located) experienced much lower current densities. Similarly, the E field analysis showed that the cardiac capture threshold, 40 V/cm, was exceeded only in the epidermis, dermis and sternum areas. It was expected to find higher E field values in the sternum area given its very high resistivity. The regions posterior to the sternum (e.g. where cardiac tissue would be located) experienced E fields significantly lower than the cardiac capture threshold.

Figure 6 shows the voltage distribution for this model. Figure 7(a) shows the resulting current density distribution. Figure 7(b) shows the same current density map with the color scheme modified to red for values that exceeded the VF threshold. Figure 8(a) shows the resulting E field distribution. Figure 8(b) shows the same E field map with the color scheme modified to red for values greater than the cardiac capture threshold. The modified color schemes reached down to very low levels of current density and E field, respectively. As such, some computational artifacts were revealed. They were not expected to be accurate reflections of the true electric field solution (e.g. the bump at the center of the E field in Fig. 8(b) or the sliver of color at the borders between abrupt tissue resistivity changes).

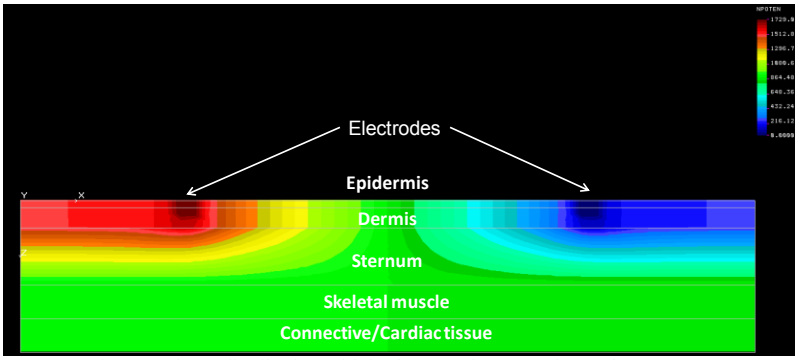

Fig. 6. Voltage distribution with both CEW darts anterior to the sternum.

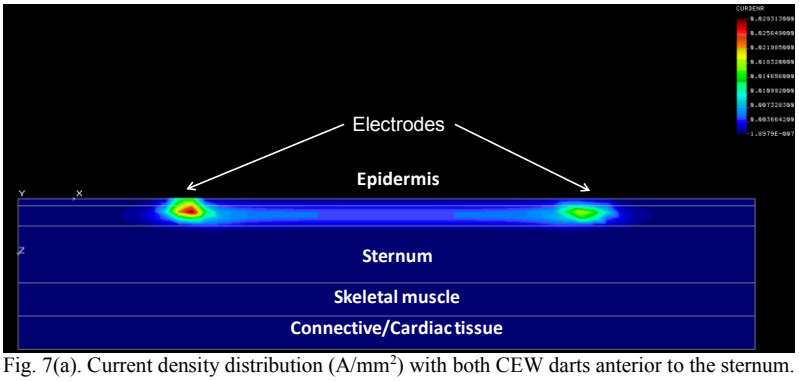

Fig. 7(a). Current density distribution (A/mm^2) with both CEW darts anterior to the sternum.

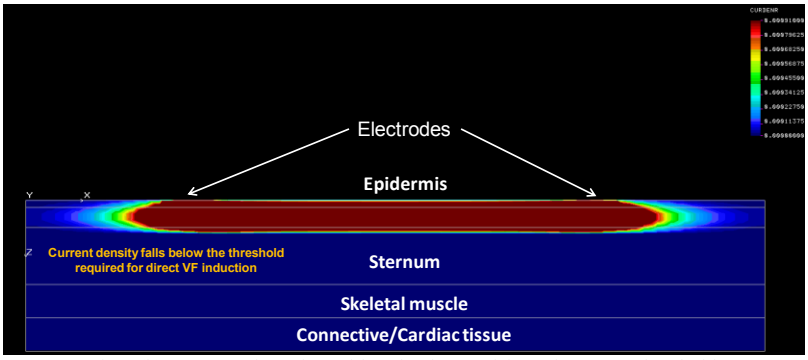

Fig. 7(b).Same as above but with red color used for values >VF threshold.

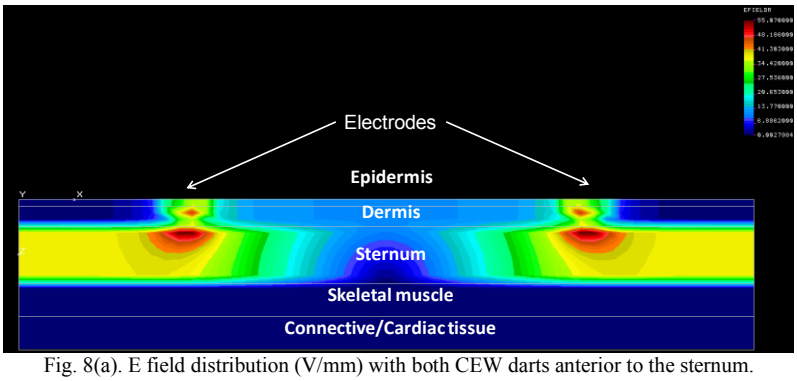

Fig. 8(a). E field distribution (V/mm) with both CEW darts anterior to the sternum.

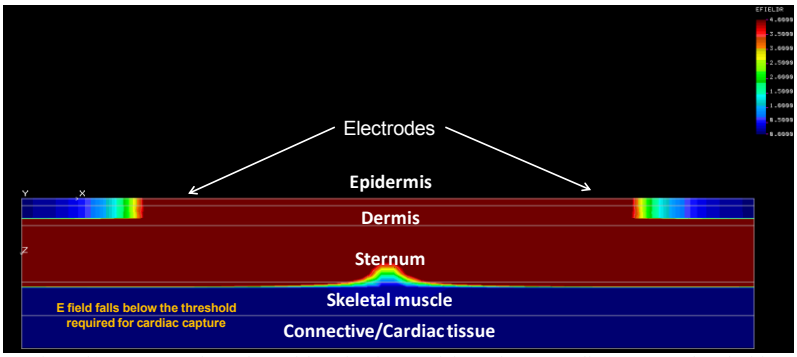

Fig. 8(b). Same as above but with red color used for values >cardiac capture threshold.

With only one CEW dart deployed anterior to the sternum, the FEM predicted that the current density will exceed the VF threshold, 91 mA/cm^2, only in the epidermis, dermis, and some anterior parts of the fat region. All regions directly posterior to the sternum (e.g. where cardiac tissue would be located) experienced much lower current densities. Similarly, the E field analysis showed that the cardiac capture threshold, 40 V/cm, was exceeded only in the epidermis, dermis, sternum and fat areas. It was again expected to find higher E field values in the sternum and fat areas given their very high resistivities. The regions directly posterior to the sternum (e.g. where cardiac tissue would be located) experienced E fields significantly lower than the cardiac capture threshold.

Figure 9 shows the voltage distribution for this model. Figure 10(a) shows the resulting current density distribution. Figure 10(b) shows the same current density map with the color scheme modified to red for values that exceeded the VF threshold. Figure 11(a) shows the resulting E field distribution. Figure 11(b) shows the same E field map with the color scheme modified to red for values greater than the cardiac capture threshold. As for the first model, the modified color schemes reached down to very low levels of current density and E field, respectively. As such, there were again some computational artifacts shown which were not expected to be accurate reflections of the true electric field solution (e.g. the non-uniform aspect of current density in the fat region in Fig. 10(b) or the sliver of color at the borders between abrupt tissue resistivity changes).

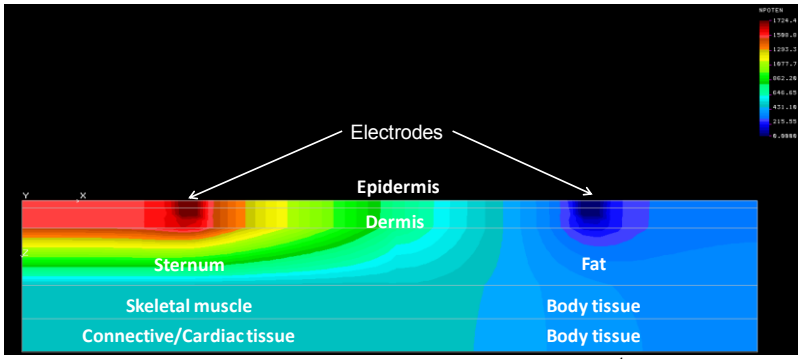

Fig. 9.Voltage distribution with a CEW dart anterior to the sternum and 2nd CEW dart at abdomen.

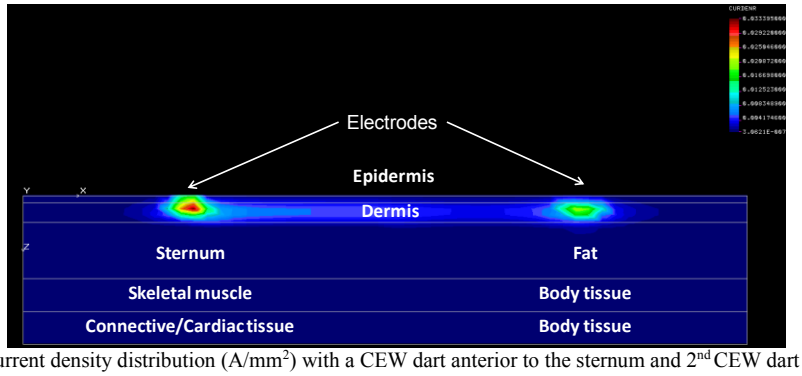

Fig. 10(a). Current density distribution (A/mm^2) with a CEW dart anterior to the sternum and 2nd CEW dart at abdomen.

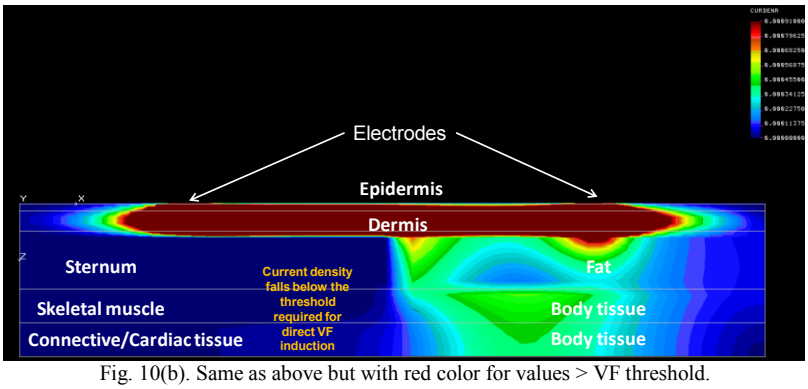

Fig. 10(b). Same as above but with red color for values > VF threshold.

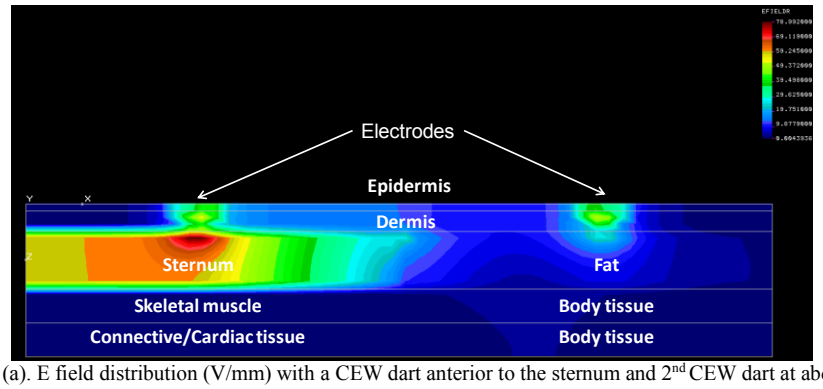

Fig. 11(a). E field distribution (V/mm) with a CEW dart anterior to the sternum and 2nd CEW dart at abdomen.

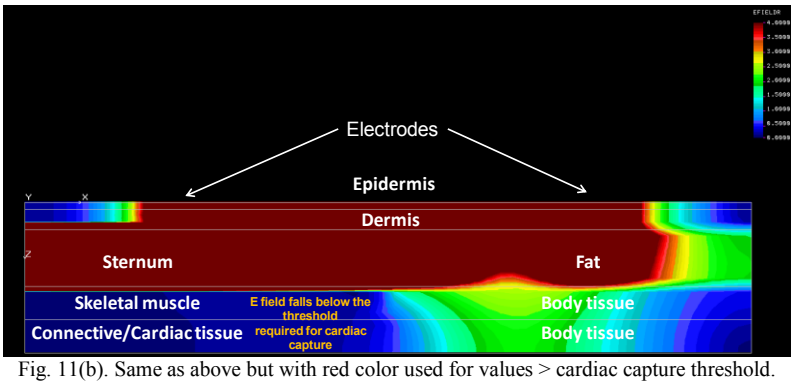

Fig. 11(b). Same as above but with red color used for values > cardiac capture threshold.

Figures 12(a) and (b) illustrate a superposition of Figs. 7(b) and 10(b) over a lateral view of a subject's torso. The illustrations are to scale, considering average human torso dimensions. It can be seen that the current density is significantly below VF thresholds at locations corresponding to the heart region. Similarly, Figs. 13(a) and (b) show a superposition of Figs. 8(b) and 11(b) over a torso lateral view. E field distributions are significantly below capture thresholds at locations corresponding to the heart.

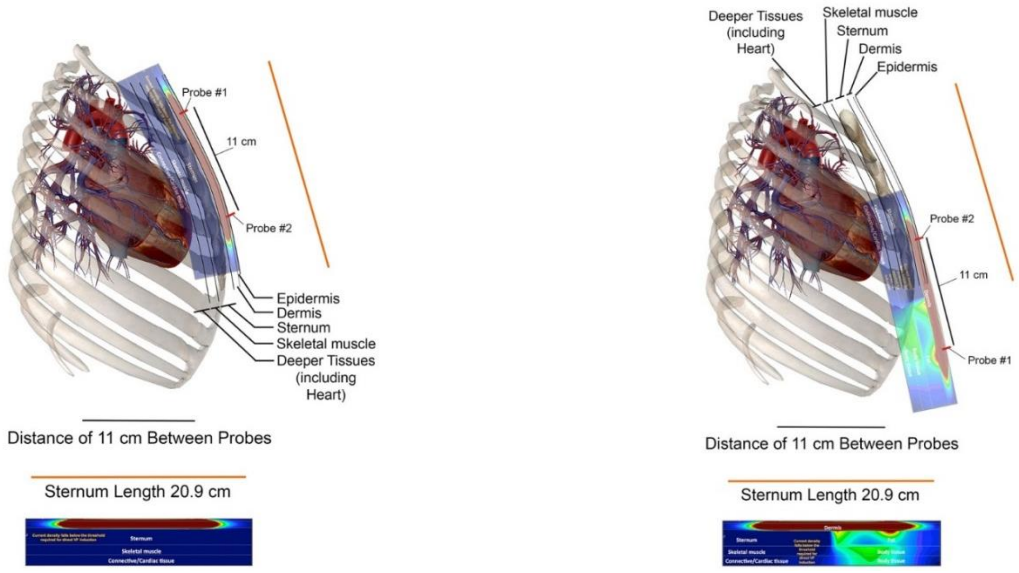

(a) (b)

Fig. 12. Current density distribution relative to heart. (a) Both CEW darts anterior to sternum; (b) one CEW dart anterior to sternum, one at abdomen.

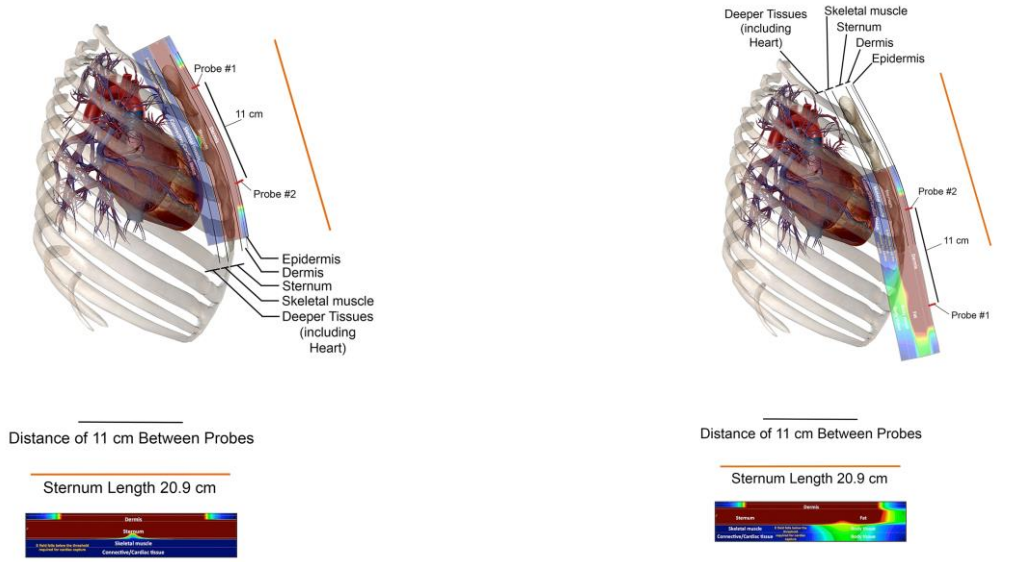

(a) (b)

Fig. 13. E field strength distribution relative to heart. (a) Both CEW darts anterior to sternum; (b) one CEW dart anterior to sternum, one at abdomen.

IV. Discussion

Emergency physicians never perform transcutaneous pacing via small electrodes placed over a patient's sternum. Use of large electrodes and other placements were found to be more efficacious [20]. Intuitively, it is therefore expected that the small CEW electrical charge delivered through its small electrodes, would be sufficiently attenuated by the presence of the sternum so as to effectively significantly reduce probabilities of myocardial stimulation.

Both of our FEMs predicted that the residual electrical current or charge from CEWs would be insufficient to cause either cardiac capture or direct induction of VF at locations where cardiac tissue would reside relative to the posterior aspect of the sternum. These findings held true even when the second CEW dart deployed farther away from the sternum. In our analyses, we assumed that the second CEW dart deployed over the abdomen. The increased resistivity of fat offered significant attenuation of CEW currents, although not as much as that caused by the sternum. We would expect similar results for second-CEW dart locations over other tissue areas of high resistivity, such as lungs, rib cage or intercostal muscle. It is well known that the thoracic cage (ribs and skeletal muscles) shunts most electrical charge and intercostal muscles display electrical anisotropy. The anisotropy can further contribute to CEW current attenuation should the darts land over such areas [20].

Future work may look into performing probabilistic analyses with intent to estimate the probability of the cardiac capture when, during actual use, CEW darts deploy anterior to the sternum.

V. Conclusion

Based on the above FEM results, we concluded that the sternum offers significant shielding effect and protects the tissues posterior to it against effects of electrical current flow from CEW electrodes positioned anterior to the sternum.

VI. Disclosure

Dr. Panescu is a paid consultant to TASER International, Inc. (TASER). Dr. Kroll is a consultant to TASER, and a member of the TASER Scientific and Medical Advisory Board (SMAB) and Corporate Board. Mr. Brave is an employee of TASER and legal advisor to the TASER SMAB and Training Advisory Board.

VII. References

[1] TASER Technology Summary. Available at http://www.taser.com/research-and-safety/science-and-medical

[2] P. W. Smith, Hand-held stun gun for incapacitating a human target, US Patent 6,636,412, October 21, 2003.

[3] TASER International: Law Enforcement Technology. Available at http://www.taser.com/products/law-enforcement

[4] D. M. Dawes, J. D. Ho, M. W. Kroll and J. R. Miner, "Electrical Characteristics of an Electronic Control Device Under a Physiologic Load: A Brief Report," *PACE*, pp. 1–7, 2009.

[5] D. Panescu, M.W. Kroll, R.A. Stratbucker, "Medical safety of TASER conducted energy weapon in a hybrid 3-point deployment mode," *Conf Proc IEEE Eng Med Biol Soc*, vol. 2009, pp. 3191-4, 2009.

[6] D. Panescu, M.W. Kroll, R.A. Stratbucker, "Theoretical probability of ventricular fibrillation induction during use of TASER neuromuscular incapacitation devices," *Conf Proc IEEE Eng Med Biol Soc,* vol. 2008, pp. 5671-4, 2008.

[7] L.A. Geddes and L. E. Baker. Principles of Applied Biomedical Instrumentation, 3rd Ed. New York: John Wiley & Sons, 1989.

[8] H. Sun. Models of ventricular fibrillation probability and neuromuscular stimulation after Taser® use in humans. PhD thesis: University of Wisconsin, 2007. Available online: http://ecow.engr.wisc.edu/cgi-bin/get/ece/762/webster/

[9] H. Sun, J. Y. Wu, R. Abdallah and J. G. Webster, "Electromuscular incapacitating device safety," *Proc IFMBE*, 3rd EMBE Conference, Prague, vol. 11(1), 2005.

[10] G. P. Walcott, B. H. KenKnight, W. M. Smith and R. K. Ideker, "Strength-Duration Curves for Ventricular Pacing and Defibrillation," *PACE*, vol. 18(II), 1995.

[11] S. B. Knisley, W. M. Smith and R. E. Ideker, "Effect of field stimulation on cellular repolarization in rabbit myocardium. Implications for reentry induction," *Circ Res*, vol. 70(4), pp. 707-715, 1992.

[12] S. B. Knisley, W. M. Smith and R. E. Ideker, "Prolongation and shortening of action potentials by electrical shocks in frog ventricular muscle," *Am J Physiol*, vol. 266(6 Pt 2), pp. H2348-2358, 1994.

[13] H. Bien, L. Yin and E. Entcheva, "Calcium instabilities in mammalian cardiomyocyte networks," *Biophys J*, vol. Jan 6, 2006.

[14] S. Singh and S. Saha, "Electrical properties of bone. A review," *Clin Orthop Relat Res*, vol. (186), pp. 249-71, 1984.

[15] J. P. Delille, A. Hernigou, V. Sene, G. Chatellier, J. C. Boudeville, P. Challande and M. C. Plainfosse, "Maximal thickness of the normal human pericardium assessed by electron-beam computed tomography," *Eur Radiol*, vol. 9(6), pp. 1183-9, 1999.

[16] H. A. M. Mahinda and O. P. Murty, "Variability in thickness of human skull bones and sternum – an autopsy experience," *J Forensic Medicine and Toxicology*, vol. 26(2), 2009.

[17] H. Gray, "Osteology" in *Anatomy of the Human Body*, 20th ed. Philadelphia: Bartleby.com, 2000.

[18] G. Mall, G. Sprinzl and J. Koebke, "Clinical morphology of the sternum," *Biomed Tech*, vol. 36, pp. 288-289, 1991.

[19] Structural Research & Analysis Corporation (SRAC), division of SolidWorks Corporation, COSMOS/M: http://www.cosmosm.com/pages/products/cosmosm.html.

[20] D. Panescu, J. G. Webster, W. J. Tompkins and R. A. Stratbucker, "Optimization of transcutaneous cardiac pacing by three-dimensional finite element modeling of the human thorax," *Med. Biol. Eng. Comput.,* vol. 33(6), pp. 769-775, 1995.